Molecularly imprinted polymer based on MWCNTs-QDs as fluorescent biomimetic sensor for specific recognition of target protein

Ding Zhaoqiang, Bligh S.W. Annie, Tao Lei, Quan Jing, Nie Huali, Zhu Limin, Gong Xiao

This is an author's accepted manuscript of an article published in the Materials Science and Engineering C, 48, 469-479, 2015. The final definitive version is available online at: https://dx.doi.org/10.1016/j.msec.2014.12.032

Molecularly imprinted polymer based on MWCNTs-QDs as fluorescent biomimetic sensor for specific recognition of target protein

Zhaoqiang Ding[a], S. W. Annie Bligh [b], Lei Tao[a] Jing Quan[a], Huali Nie[a, 1], Limin Zhu[a, *], Xiao Gong[a]

[a] *College of Chemistry, Chemical Engineering and Biotechnology, Donghua University, Shanghai 201620, P.R. China*

[b] *Department of Life Sciences, Faculty of Science and Technology, University of Westminster, 115 New Cavendish Street, London W1W 6UW, UK.*

Abstract

In this work a novel molecularly imprinted optosensing material based on multi-walled carbon nanotubes-quantum dots (MWCNTs-QDs) was synthesized for highly selective and sensitive specific recognition of the target protein bovine serum albumin (BSA). Molecularly imprinted polymer coated MWCNTs-QDs using BSA as the template (BMIP-coated MWCNTs-QDs) exhibited a fast mass-transfer speed (the response time was 25 min). It was found that the BSA as target protein can remarkably quench the luminescence of BMIP-coated MWCNTs-QDs in a concentration-dependent manner that was best described by a Stern-Volmer equation. The K_{SV} for template BSA was much higher than bovine hemoglobin (BHb) and lysozyme (Lyz), implying a highly selective recognition ability of the BMIP-coated MWCNTs-QDs to BSA. Under optimal conditions, the relative fluorescence intensity of BMIP-coated MWCNTs-QDs decreased linearly with the increasing target protein BSA in the concentration in the range of 5.0×10^{-7} - 35×10^{-7} M with a detection limit of 80 n M.

Keywords: Protein recognition; Fluorescent biomimetic sensor; Molecularly imprinted polymer; Multi-walled carbon nanotubes; Quantum dots

* Corresponding authors. Tel.: +86 21 6779 2748; fax: +86 21 6237 2655. E-mail addresses: lzhu@dhu.edu.cn (L.-M. Zhu); niehuali@dhu.edu.cn (H.-L. Nie).

1. Introduction

With the rapid development of proteomics research, better understanding of the structure function of living organisms at the molecular level through studying the function of newly discovered proteins in cells is highly significant.[1-2] Proteomics involves the detection and identification of proteins concentration of which can cover a very wide range. Traditionally, it is very difficult to detect low abundance proteins that often have significant biological functions in the presence of high concentrations of other components. The classical method of immunoassay employs antibodies which usually have several fundamental limitations including chemical and physical instability, unease of preparation, and high manufacturing cost.[3] In this respect, alternative artificial biomimetic receptors, such as molecularly imprinted polymers (MIP), exhibit unique potential to apply in the field of protein recognition.[4-6] MIP, generally prepared by molecularly imprinted technique (MIT), is a synthetic material with an artificially generated three-dimensional network that can re-bind to specific target molecule.[7-10] Protein-imprinted materials have specific recognition sites formed through interaction with template proteins, which direct the positioning and orientation of the structural components of the materials.[5-6] While the imprinting of small molecules is straightforward, the preparation of MIP against biomacromolecules, such as proteins, still remains some challenges due to the features of the protein such as large molecular size, flexible structure and many functional groups.[2, 11-12] Therefore, it is vital to develop highly selective and efficient analytical approach for identifying and quantifying proteins through MIT. Protein-imprinting can be divided in several categories including bulk[13], particle[14-15], epitope or aspira partial[16], and surface imprinting[17-19]. Among the approaches above, surface imprinting offers unique potentials, which is achieved by attaching the protein template to the surface of a substrate (flat or spherical) with subsequent polymerization around it. This technique successfully places binding cavities on or near the substrate surfaces, solving the problems of restricted mass transfer and facilitating removal of the template, but the density of surface binding sites is still limited due to the small surface area to volume ratio of these conventional MIP.[17-18]

Nanomaterials, which possess unique characteristics of large surface-to-volume ratio and size-related physical and chemical properties, are now among the most researched alternatives to overcome the drawbacks associated with conventional MIP. Recently, molecular imprinting of nanomaterial surfaces

has been extended to the imprinting of proteins. These nanostructured MIPs enable complete removal of templates, better site accessibility, reduction of effect of mass transfer resistance, and have a well-defined shape.[20-21]

Quantum dots (QDs), also known as semiconductor nanocrystals, have found preliminary applications in optical and electronic devices[22-23], chemical sensors[24], light emitting diodes[25-26], photovoltaic devices[27-28] and biological imaging and sensing[29-35] due to the unique chemical, physical and optical properties. The combination of QDs with highly selective MIP has recently attracted considerable attention as the composite materials exhibiting both highly specific recognition from MIP and sensitive signal amplification and optical readout characteristic from QDs.[36-37] Although these materials have distinctive advantages, there are still some drawbacks such as long response time and poor fluorescence signal stability.

Herein we design and synthesize a novel molecularly imprinted optosensing materials based on multi-walled carbon nanotubes-QDs (MWCNTs-QDs) attempting to overcome the above disadvantages. While the composites of MWCNTs-QDs have exhibited enhanced photocatalysis and photocurrent in electrochemical sensing, very little attention has been paid to optosensing determination of analytes, especially for protein. Why would MWCNTs be applied into this study? MWCNTs have been extensively exploited for biomedical applications due to their unique intrinsic physical and chemical properties. Moreover, MWCNTs have been considered as an ideal matrix for the synthesis of MWCNTs-based nanohybrids for biomedical applications because of their large surface area to load nanoparticles in a one-dimensional direction, preventing the aggregation of nanoparticles in solution.[38-41] The utilization of MWCNTs as building blocks for nanodevices can readily be realized. Therefore, by combining the attractive tubular structure with its fluorescent property, the QD-decorated carbon nanotube can be an ideal candidate for a multifunctional nanomaterial.[42-43] To improve the solubility and stability of the MWCNTs in aqueous phase, polyethylenimine (PEI) was chosen to modify carboxylated MWCNTs to obtain PEI functionalized MWCNTs (PEI-MWCNTs) through a covalent connection approach. Hetero-junctions of QDs and MWCNTs could become better alternatives for the synthesis of nanoscale devices. The introduction of CdTe/CdS QDs nanoparticles to the sidewalls of MWCNTs is achieved through the formation of covalent bonds between MWCNTs and QDs. Then the fluorescence sensor to target protein

bovine serum albumin (BSA) was accomplished by protein-imprinting based on the MWCNTs-QDs nanohybrids *via* sol-gel method.

The response of the intensity of fluorescence signal and the application capability of BMIP-coated QDs (molecularly imprinted polymer coating CdTe/CdS QDs using BSA as the template) and BMIP-coated MWCNTs-QDs (molecularly imprinted polymer coating MWCNTs-QDs nanohybrids using BSA as the template) were researched in a series of experiments including adsorption capacity study, time-dependent fluorescence responses, optosensing of protein as well as specific study.

2. Materials and methods

2.1 Materials and chemicals

All chemicals were analytical grade reagents. Tellurium powder (Te), $CdCl_2 \cdot 2.5H_2O$, $NaBH_4$, thioacetamide (TAA) and 3-mercaptopropionic acid (MPA) as the capping agent were purchased from Sinopharm Chemical Reagent Co., Ltd to prepare CdTe/CdS QDs. Carboxylated MWCNTs were purchased from the Chinese Academy of Science, Chengdu Organic Chemistry Co., Ltd. N-(3-dimethylaminopropyl)-N'-ethylcarbodiimide hydrochloride (EDC·HCl), N-hydroxysuccinimide (NHS)□ polyethylenimine (PEI) and dimethyl sulfoxide (DMSO) were purchased from Sinopharm Chemical Reagent Co., Ltd to prepare PEI-MWCNTs and MWCNTs-QDs nanohybrids. Tetraethoxysilane (TEOS), 3-aminopropyltriethoxysilane (APTES), $NH_3 \cdot H_2O$ and Triton X-100 (Tri) were got from Sinopharm Chemical Reagent Co., Ltd to synthesize protein imprinted silica shell. Bovine serum albumin (BSA, 68 kDa, pI 4.9), lysozyme (Lyz, 14.4 kDa, pI 10.8) and bovine hemoglobin (BHb, 66 kDa, pI 6.7) were obtained from Sigma-Aldrich Co. (St. Louis, MO).

2.2 Characterization

Fluorescence measurements were performed on a QM/TM spectrofluorometer (PTI, USA) equipped with a 1×1 cm^2 quartz cell. The slit widths of the excitation and emission were both 3.0 nm, and the excitation wavelength was set at 380 nm. Confocal laser scanning microscopy (Carl Zeiss LSM 700, Jena, Germany) was used to study the luminescence behavior of the fluorescent materials. Ultraviolet-visible (UV-vis) spectra (200-800 nm) were recorded on a Lambda 35 spectrophotometer (PerkinElmer, USA). Morphology and composition of the materials were characterized using high resolution transmission electron microscopy (HRTEM) and energy dispersive spectrometer (EDS) on a JEM-2100F microscope

(JEOL, Tokyo, Japan). Transmission electron microscope (TEM) images were obtained on a JEM-2100 microscope (JEOL, Tokyo, Japan). Fourier transform infrared (FT-IR) spectra (4000-400 cm^{-1}) in KBr were recorded on a Nicolet 6700 FT-IR spectrometer (Thermo Fisher, USA).

2.3 Preparation of CdTe, CdTe/CdS QDs and MWCNTs-QDs

The water-soluble CdTe/CdS QDs were synthesized on the basis of a previous publication with slight modifications.[44] For the preparation of MPA-capped CdTe cores, 0.25 mmol $CdCl_2 \cdot 2.5H_2O$ and 52 μL (0.6 mmol) MPA were dissolved in 200 mL of water to get a precursor solution followed by adjusting the pH value to 8.5 using 1 M NaOH solution. After N_2 was bubbled through the solution for 30 min, 4 mL of freshly prepared NaHTe solution from $NaBH_4$ (0.75 mmol) and Te (0.375 mmol) powder was added to the above precursor solution under continuous stirring. Finally, the complex solution with a faint yellow color was refluxed at 100°C for 60 min. The as-prepared CdTe solution was concentrated to a quarter of the original volume and CdTe QDs were precipitated with 2-propanol and collected using centrifugation. The colloidal precipitate was re-dissolved in ultrapure water (3 mL) and used as CdTe core to inject into the N_2 saturated CdS solution (200 mL) containing 0.25 mmol $CdCl_2 \cdot 2.5H_2O$, 0.25 mmol TAA and 1.2 mmol MPA (pH 8.5) under stirring, and the solution was heated up until boiling. Under reflux, fluorescence of the solution appeared and could be tuned in color by prolonging the refluxing time. After being refluxed for 60 min, MPA stabilized CdTe/CdS QDs exhibiting strong fluorescence were obtained. The as-prepared CdTe/CdS solution was concentrated to a quarter of the original volume and CdTe/CdS QDs were precipitated with 2-propanol and collected using centrifugation. The colloidal precipitate was re-dissolved in ultrapure water and used in the next step.

A typical synthesis of MWCNTs and CdTe/CdS QDs nanohybrids was as follows. Firstly, the as-received MWCNTs-COOH were covalently functionalized with PEI under sonication for 24 h using EDC·HCl as coupling agent in DMSO solution. The obtained PEI-MWCNTs solution was dialyzed for 3 days to remove excess chemicals. Secondly, the as-prepared CdTe/CdS solution was added to EDC·HCl/NHS mixture solution in a molar ratio of 1:1, and stirred for 30 min to activate the carboxyl groups on the surface of CdTe/CdS QDs. Moreover, PEI-MWCNTs were added into the above-mentioned solution under sonication for 24 h to covalently couple CdTe/CdS QDs onto the surface of the PEI-MWCNTs, denoted as MWCNTs-QDs nanohybrids.[45]

2.4 Synthesis of fluorescent BSA imprinted artificial sensors

BMIP-coated QDs were prepared based on the previous report [46], to a 50 mL flask, 20 mg of template protein BSA, 20 mL of CdTe/CdS QDs and 80 μL of APTES were added and stirred for 30 min. TEOS (120 μL) followed by 200 μL of the $NH_3 \cdot H_2O$ ((w/v) 25%) were added and stirred for a further 12 h at room temperature. After the reaction, the resultant BMIP-coated QDs were centrifuged and washed with deionized water to remove the absorbed oligomers and unreacted monomers. The BMIP-coated QDs were then washed repeatedly with 0.5% Tri to remove the template until no BSA in the supernatant was detected at λ = 280 nm by UV-vis spectroscopy. Finally, the precipitate of BMIP-coated QDs were re-dispersed in phosphate buffer solution and then stored at 4 °C prior to use. The non-imprinted polymer coated QDs (NIP-coated QDs) were synthesized in parallel but without the addition of the template molecule.

BMIP-coated MWCNTs-QDs were prepared as follows: to a 50 mL flask, template protein BSA (20 mg), MWCNTs-QDs nanohybrids (20 mg), APTES (80 μL) and water (20 mL) were added and stirred for 30 min. Then, TEOS (120 μL) was added. Next, 200 μL of the $NH_3 \cdot H_2O$ ((w/v) 25%) was added and stirred for 12 h in room temperature. After the reaction, the resultant BMIP-coated MWCNTs-QDs were centrifuged and washed with deionized water to remove the absorbed oligomers and unreacted monomers. Then the BMIP-coated MWCNTs-QDs were washed with 0.5% Tri, which was repeated several times until no template was detected by UV-vis spectroscopy at λ = 280 nm. Finally, the precipitate of BMIP-coated MWCNTs-QDs were re-dispersed in phosphate buffer solution and then stored at 4 °C prior to use. The NIP-coated MWCNTs-QDs were prepared using the same procedure but without the addition of the template molecule.

3. Results and discussion

3.1 Synthesis and characterization of BSA imprinted artificial sensors

The design of the sensor of BMIP-coated MWCNTs-QDs is based on the fact that the MWCNTs-QDs nanohybrids act as antennae for recognition signal amplification and optical readout, while the MIP shell provides analyte selectivity and prevents interfering molecules from coming into contact with the antennae. Scheme for synthesizing BMIP-coated MWCNTs-QDs was shown in Fig. 1. The MIP silica shell was prepared *via* a surface molecularly imprinting technique.[47] In this sol-gel reaction, APTES was

used as a functional monomer which had a non-covalent interaction with the template protein to form the complexes. Then the resultant complexes were reacted with TEOS which was used as the cross-linker and $NH_3 \cdot H_2O$ as a catalyst to accelerate the reaction process. The resultant silica shell was an ideal polymeric material with highly rigid matrix and hydrophilic surface. After eluting the template molecules, recognition cavities complementary to the template molecule in shape, size, and chemical functionality were formed in the cross linked polymer matrix. BMIP-coated QDs was prepared using the same procedure replacing MWCNTs-QDs with CdTe/CdS QDs.

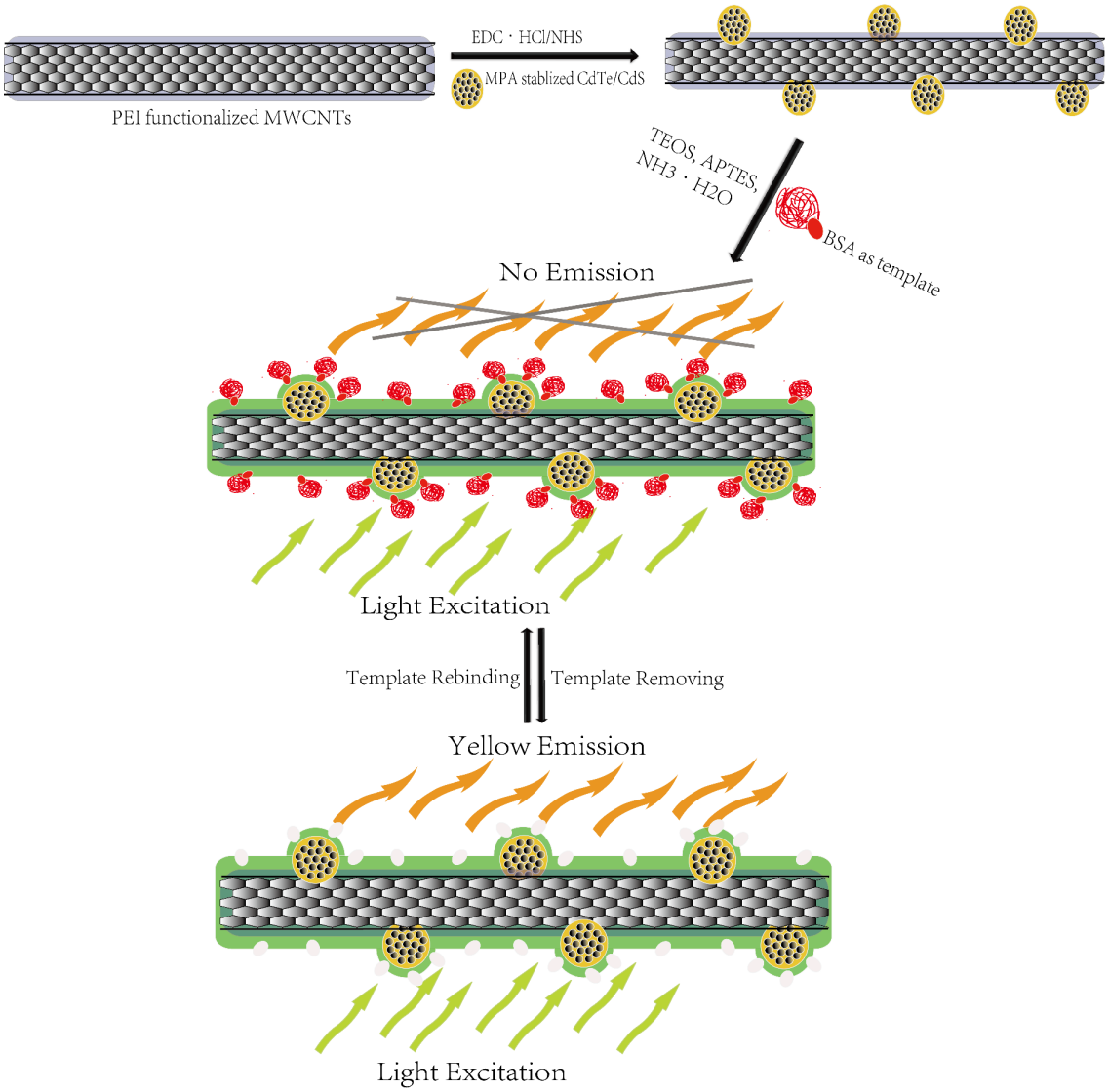

Fig. 1 Schematic illustration for the preparation of biomimetic sensor BMIP-coated MWCNTs-QDs.

Before synthesis of MIP shell on the surface of the nanohybrids, we prepared the CdTe/CdS QDs and

MWCNTs-QDs nanohybrids firstly. Most of the artificial sensors, reported so far, were prepared based on CdTe QDs which exhibited poor optical properties.[48] In addition, it also required a longer time to obtain CdTe QDs with a long emission peak wavelength using an aqueous strategy. It was necessary to construct a CdS shell on the surface of CdTe core to improve the luminescent stability and robustness of the QDs. Moreover, it could reduce the synthesis time to obtain the CdTe/CdS QDs with a long emission peak wavelength as well as excellent optical properties. As shown in Fig. 2(a) and (d), compared to that of CdTe QDs, the fluorescence band of CdTe/CdS QDs shifted to 574 nm from 520 nm of CdTe QDs within 120 min of refluxing time. For MWCNTs-QDs, firstly MWCNTs were covalently functionalized with PEI with amine groups being terminated on their surface (more details were shown in Fig. S1). Then the carboxyl modified CdTe/CdS QDs were attached on the surface of the PEI-MWCNTs by a dehydration reaction between the amine and carboxyl moieties using EDC·HCl/NHS as agents. Fig. 2(a) and (e) also showed the fluorescence spectra and confocal fluorescence image of MWCNTs-QDs nanohybrids. The MWCNTs-QDs exhibited a strong emission band at 576 nm and shifted about 2 nm upwards comparing to that of free CdTe/CdS QDs. This effect was also observed in other CNT-QDs nanohybrids.[49-51] It is believed that the redshift was probably caused by a decreased quantum confinement of QDs and a different surrounding environment of QDs in the MWCNTs-QDs nanohybrids.

Fig. 2(b) showed fluorescence spectra of BMIP-coated QDs, NIP-coated QDs and BMIP-coated QDs with template BSA. The fluorescence intensity of BMIP-coated QDs was quenched when the template was re-bound to the MIP, after the template was extracted from the composites and the fluorescence intensity of BMIP-coated QDs recovered. Fluorescence spectra of BMIP-coated MWCNTs-QDs, NIP-coated MWCNTs-QDs and BMIP-coated MWCNTs-QDs with template BSA were shown in Fig. 2(c). Similarly, the fluorescence intensity of BMIP-coated MWCNTs-QDs was also quenched when the template was re-bound to the sensors, after the template was extracted from the composites and the fluorescence intensity of BMIP-coated MWCNTs-QDs recovered. It could be seen from Fig. 2(a), (b), (c) that there were red-shift of the emission peak after the formation of silica shell on the surface of the QDs and nanohybrids (578 nm of BMIP-coated QDs from 574 nm of CdTe/CdS QDs, 582 nm of BMIP-coated MWCNTs-QDs from 576 nm of MWCNTs-QDs). This was due to the reduction of quantum size effect by the silica shell, thus causing a red-shift of the photoluminescence maximum.[52] Moreover, the

confocal fluorescence images clearly exhibited a strong yellow light between 570 and 590 nm in all QDs products prepared in this study.

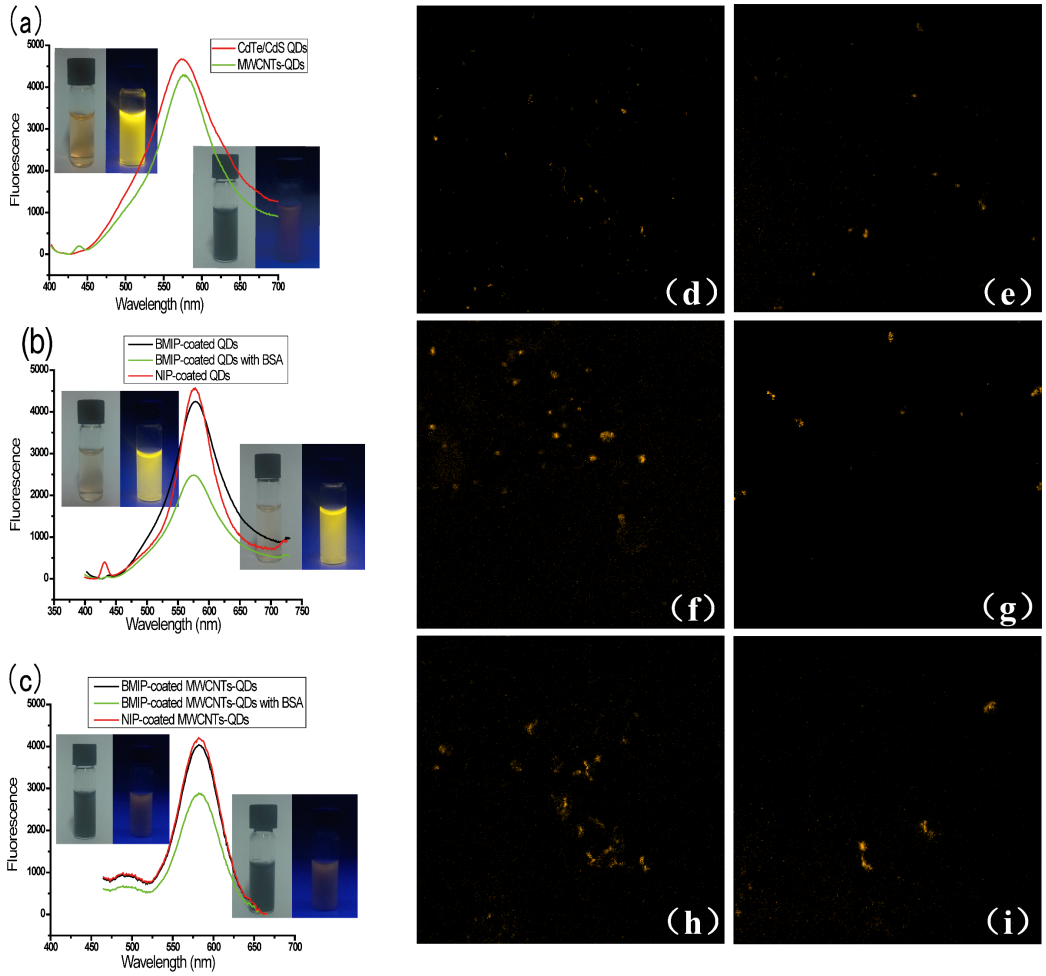

Fig. 2 (a) Fluorescence spectra of CdTe/CdS QDs and MWCNTs-QDs, insets top left were photographs of CdTe/CdS QDs in water, insets bottom right were photographs of MWCNTs-QDs in water, at room light and under UV light irradiation (λ= 365 nm); (b) Fluorescence spectra of BMIP-coated QDs, NIP-coated QDs and BMIP-coated QDs with template BSA, insets top left were photographs of BMIP-coated QDs, insets bottom right were photographs of NIP-coated QDs, at room light and under UV light irradiation (λ= 365 nm); (c) Fluorescence spectra of BMIP-coated MWCNTs-QDs, NIP-coated MWCNTs-QDs and BMIP-coated MWCNTs-QDs with template BSA, insets top left were photographs of BMIP-coated MWCNTs-QDs, insets bottom right were photographs of NIP-coated MWCNTs-QDs, at room light and under UV light irradiation (λ= 365 nm); Confocal fluorescence images of CdTe/CdS QDs (d), MWCNTs-QDs (e), BMIP-coated QDs (f), NIP-coated QDs (g), BMIP-coated MWCNTs-QDs (h) and NIP-coated

MWCNTs-QDs (i).

The TEM images of the CdTe/CdS QDs, MWCNTs-QDs, BMIP-coated QDs, and BMIP-coated MWCNTs-QDs were presented in Fig. 3(A). As shown in Fig. 3(A) (a) and (b), the CdTe/CdS QDs and BMIP-coated QDs were spherical in shape and nearly uniform in size, and the diameter of the silica nanospheres embedded QDs was about 70-80 nm. Fig. S1(a) and (b) showed the morphological and structural characterization of the PEI-MWCNTs before CdTe/CdS QDs were attached onto the surface of the PEI-MWCNTs. From Fig. S1(a) of the PEI-MWCNTs, the entangling degree was very much reduced, with a large percentage of individual nanotubes being present. Fig. S1(b) showed that MWCNTs were fully covered by a uniform amorphous polymer layer after the PEI functionalization. The MWCNTs-QDs nanohybrids were obtained through attaching CdTe/CdS QDs onto the surface of the PEI-MWCNTs (Fig. 3(A) (c)). Fig. 3(A) (d) showed the morphology of the prepared BMIP-coated MWCNTs-QDs .

The EDS measurements (Fig. 3(B)) of BMIP-coated QDs, NIP-coated QDs, BMIP-coated MWCNTs-QDs and NIP-coated MWCNTs-QDs revealed that C, O and Si were present. These results indicated that the copolymers were generated from the sol-gel condensation of APTES and TEOS.

FT-IR spectra of BMIP-coated QDs, NIP-coated QDs, BMIP-coated MWCNTs-QDs and NIP-coated MWCNTs-QDs were shown in Fig. 3(C). The strong and broad peak at around 1068 cm^{-1} indicated the Si-O-Si asymmetric stretching. The moderate peak at around 789 cm^{-1} was ascribed to the vibration of Si-O groups. The bands at around 2941 cm^{-1} were the C-H stretching bands. The peaks at around 3230 cm^{-1} and 1540 cm^{-1} were ascribed to N-H stretching band, suggesting the presence of APTES in the obtained MIP. The presence of all these bands showed that the MIP generated from sol-gel condensation was grafted on the surface of the QDs or MWCNTs-QDs nanohybrids.

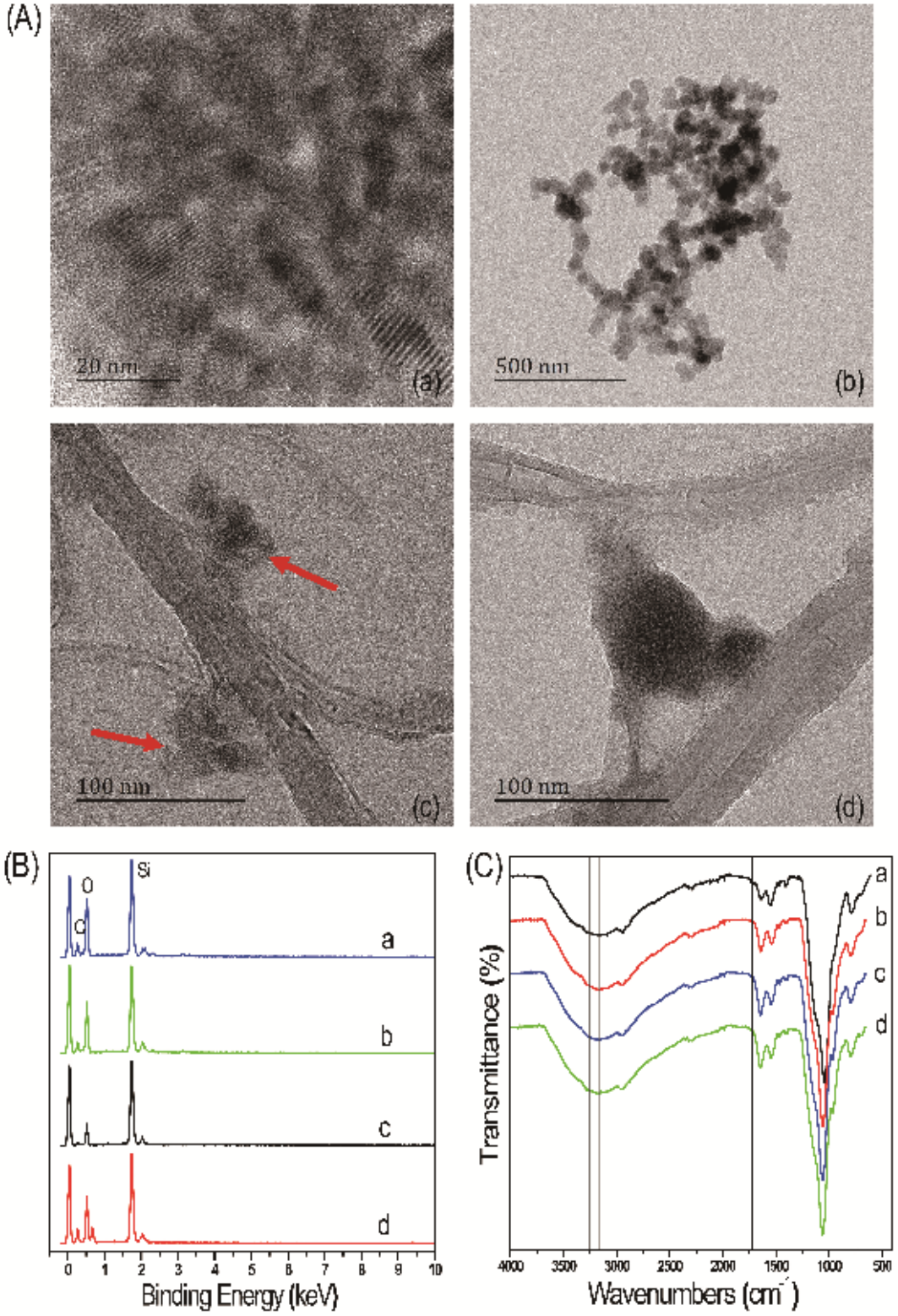

Fig. 3 (A) TEM images of the synthesized CdTe/CdS QDs (a), BMIP-coated QDs (b), MWCNTs-QDs (c), the red

arrows indicating the QDs and BMIP-coated MWCNTs-QDs (d); (B) EDS spectra and (C) FT-IR spectra of the synthesized BMIP-coated QDs (a), NIP-coated QDs (b), BMIP-coated MWCNTs-QDs (c) and NIP-coated MWCNTs-QDs (d).

3.2 Adsorption capacity of BSA imprinted artificial sensors for detection of target protein

The study of fluorescence responses of BMIP-coated MWCNTs-QDs, BMIP-coated QDs, NIP-coated MWCNTs-QDs and NIP-coated QDs with increasing concentrations of the target protein BSA were carried out. A constant amount of the composites were incubated with the increasing concentrations of BSA to equilibrate for 60 min at room temperature. As shown in Fig. 4(a), there is a relatively stable fluorescence quenching percentage in the range of 0.1 - 0.7 mg/mL of the target protein BSA. Among all the composites, BMIP-coated MWCNTs-QDs showed the strongest fluorescence quenching, indicating a high affinity between the sensor and BSA. The time responses of the sensors were also investigated to see how the MWCNTs influenced the recognition ability of the sensors after MWCNTs were applied in the composites. As shown in Fig. 4(b), there was an immediate decrease in fluorescence intensity after the addition of BSA to the four composites solutions. Compared to the NIP-coated composites, the BMIP-coated QDs showed a significant initial decrease in fluorescence intensity, but it took around 36 min to obtain a stable fluorescence intensity, indicating that the system had reached adsorption-desorption equilibrium . However, it took only about 25 min for BMIP-coated MWCNTs-QDs to obtain stable intensities, which was lower than the stable point for BMIP-coated QDs, indicating a strong fluorescence quenching due to the interaction between BSA and this sensor. The faster mass-transfer speed of BMIP-coated MWCNTs-QDs can be ascribed to the high volume of efficient surface area and high target recognition efficiency of the MWCNTs-QDs nanohybrids. Thus the response time of BMIP-coated MWCNTs-QDs as well as NIP-coated composites were set at 25 min and that of BMIP-coated QDs at 40 min.

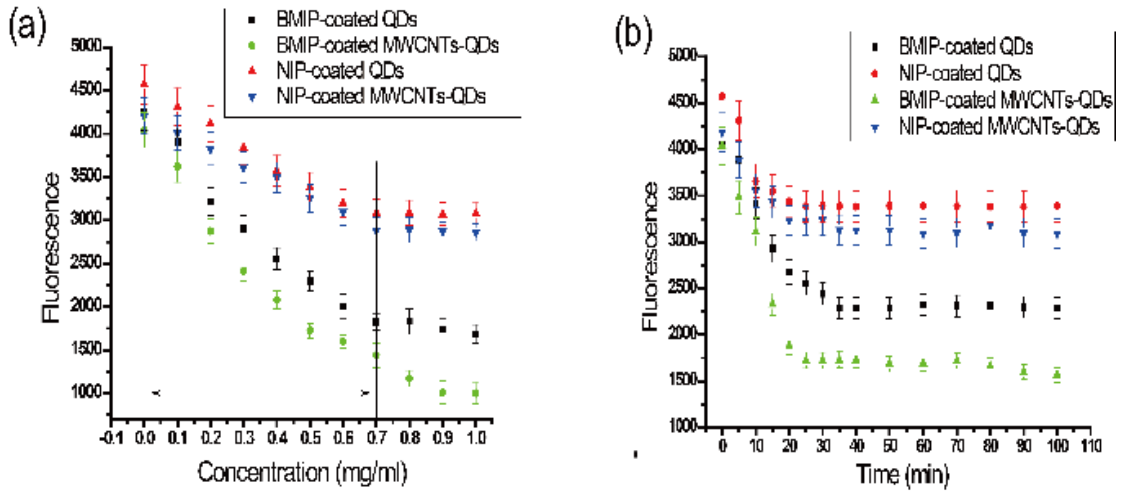

Fig. 4 (a) Fluorescence responses of BMIP-coated MWCNTs-QDs, BMIP-coated QDs, NIP-coated MWCNTs-QDs and NIP-coated QDs with increasing concentrations of BSA in the range of 0.1 - 1.0 mg/mL; (b) Time-dependent fluorescence responses of BMIP-coated MWCNTs-QDs, BMIP-coated QDs, NIP-coated MWCNTs-QDs and NIP-coated QDs in the presence of BSA (0.5 mg/mL).

3.3 Optosensing of target protein by BSA imprinted artificial sensors

It could be seen from Fig. 5 and Fig. 6 that the fluorescence intensity of the sensors was quenched gradually with the increasing concentration of template protein BSA. Generally, the fluorescence quenching in the system followed the Stern-Volmer equation as shown in the insets of Fig. 5,

$$F_0 / F = 1 + \mathrm{K_{SV}} C_q \qquad (1)$$

where F_0 was the initial fluorescence intensity in the absence of quencher, F was the fluorescence intensity in the presence of quencher, $\mathrm{K_{SV}}$ was the quenching constant of the quencher, and C_q was the concentration of the quencher. The different quenching constant was determined through the Stern-Volmer equation (1).[53] As shown in Fig. 5 and Fig. 6, the difference of linear Stern-Volmer relationships was observed between MIP and NIP, and the decrease of fluorescence intensity BMIP-coated sensors was much larger than that of the NIP-coated composites due to the presence of the quencher. For the BMIP-coated sensors, the fluorescence quenching was mainly achieved due to the specific interactions of the imprinted cavities with the template protein. In the case of the NIP, there were no specific binding sites left in the NIP-coated composites, so no obvious changes of fluorescence intensity of NIP-coated composites for target protein BSA were observed in the binding process. The changes in fluorescence intensity of the BMIP-coated MWCNTs-QDs for target protein BSA were much more obvious than the

sensor of BMIP-coated QDs. It could be predicted that much more recognition binding sites were left in the sensor of BMIP-coated MWCNTs-QDs than the other sensor and these enable imprinted cavities to selectively bind the target protein BSA. The ratio of K_{SV} of the MIP and NIP was defined as the imprinting factor (IF) to evaluate the selectivity of the sensors. For the two sensors, IF_1 of the BMIP-coated MWCNTs-QDs was 4.17, which was higher than IF_2 (2.70) of the BMIP-coated QDs, demonstrating the remarkable enhancement of the imprinting effect for the BMIP-coated MWCNTs-QDs.

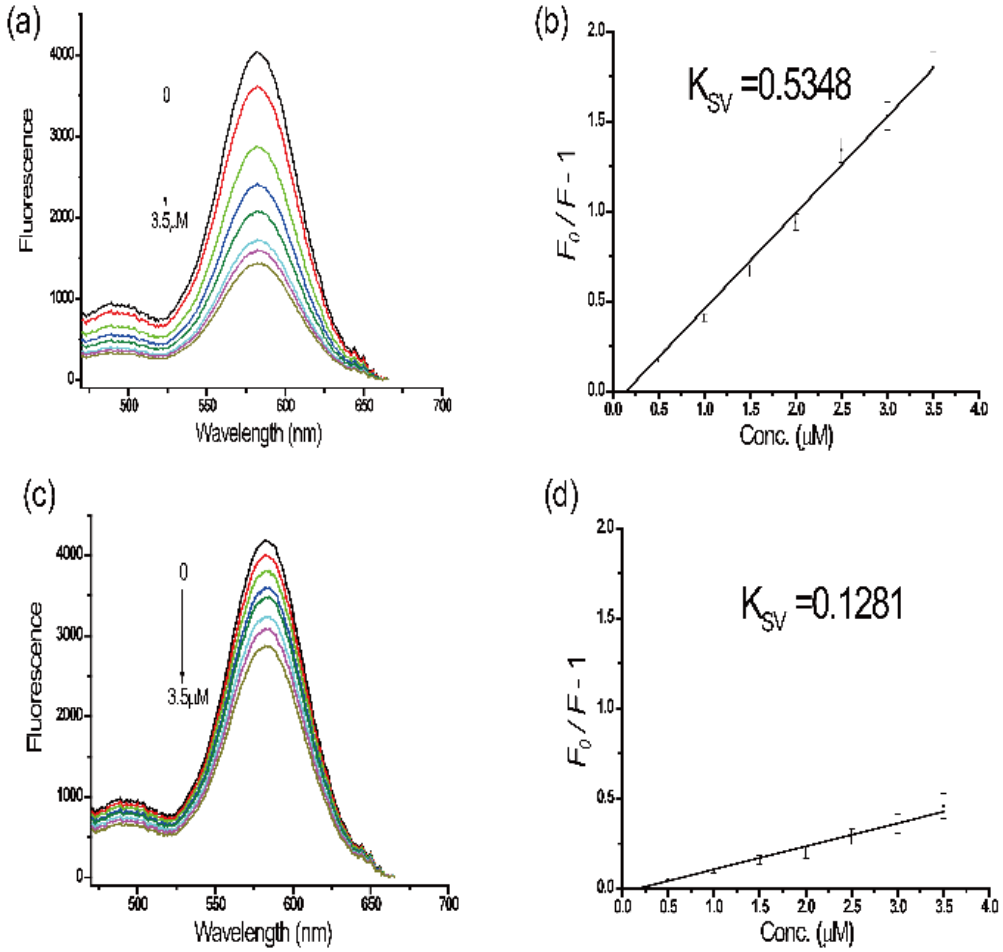

Fig. 5 Fluorescence emission spectra of (a) BMIP-coated MWCNTs-QDs and (c) NIP-coated MWCNTs-QDs; Stern-Volmer plots from (b) BMIP-coated MWCNTs-QDs and (d) NIP-coated MWCNTs-QDs with the target protein BSA.

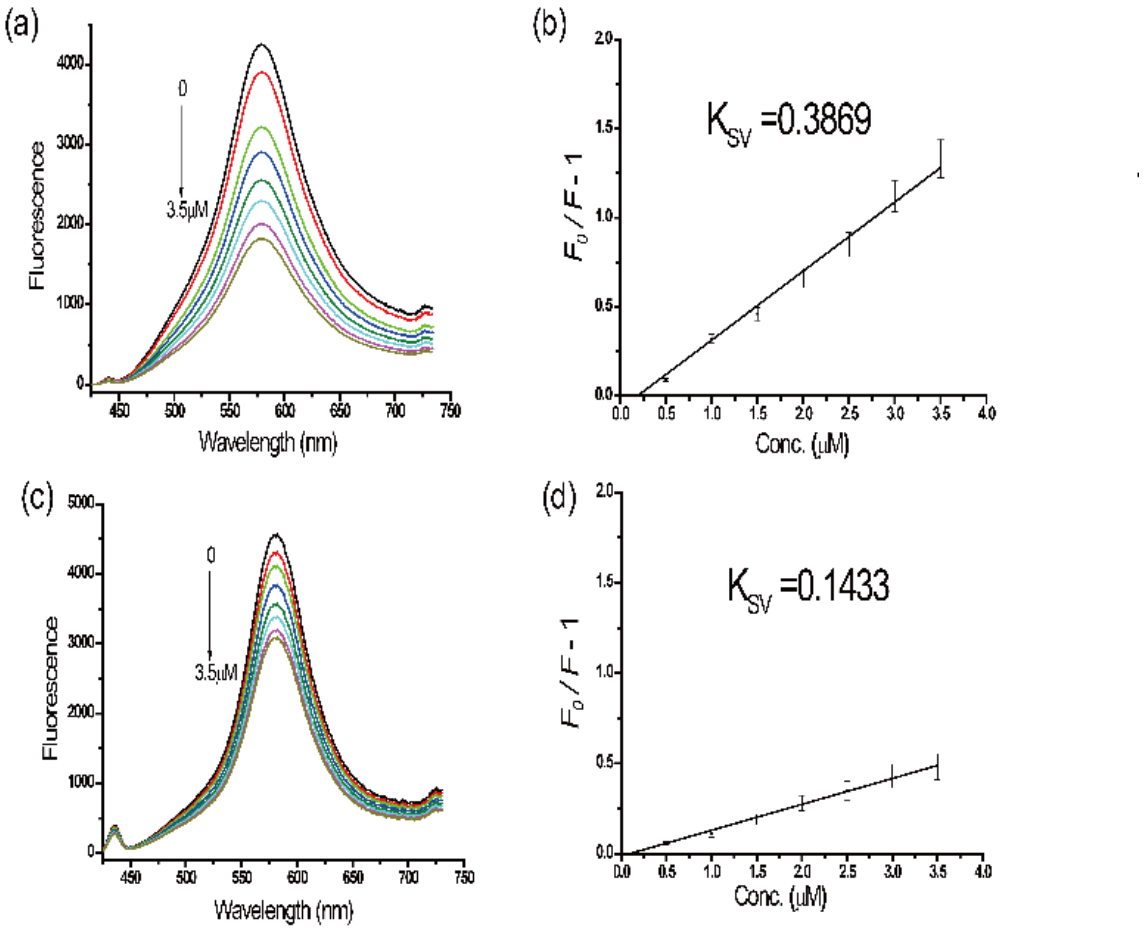

Fig. 6 Fluorescence emission spectra of (a) BMIP-coated QDs and (c) NIP-coated QDs; Stern-Volmer plots from (b) BMIP-coated QDs and (d) NIP-coated QDs with the target protein BSA.

3.4 Specificity study

To evaluate the selectivity of the sensors to the template BSA, several common proteins such as BHb and Lyz were selected for this specificity study. The linear Stern-Volmer relationships obtained for these proteins interacting with BMIP-coated or NIP-coated composites were shown in Fig. S3. The changes of fluorescence intensity of the fluorescence probes for template BSA were more obvious than its competitors of BHb and Lyz (shown in Fig. S3(a)). As shown in Fig. 7(a), the K_{SV} of BMIP-coated MWCNTs-QDs for template BSA was determined to be 0.5348, which was larger than that of 0.1098 and 0.0876 for BHb and Lyz respectively. Meanwhile, the BMIP-coated MWCNTs-QDs exhibited larger K_{SV} for the template BSA than that of BMIP-coated QDs. The K_{SV} of BMIP-coated QDs for BSA was 0.3869, which was larger than that of BMIP-coated QDs for BHb (Ksv=0.1512) and Lyz (Ksv=0.1019). Although Lyz is small enough to get into the recognition sites, the imprinted cavities are not complementary to the

Lyz, so it is unlikely to quench the fluorescence of the sensors. For the protein of BHb, although its molecule weight is close to that of BSA, its size□shape and functionality are not complementary to the recognition cavities. The results showed that the interaction intensity between BHb (or Lyz) and the imprinted cavities was much weaker than that of the template BSA. From Fig. S3(b) and Fig. 7(a) it could be seen that the changes in fluorescence intensity of NIP-coated composites were similar for BSA and its competitors BHb and Lyz (the K_{SV} of NIP-coated MWCNTs-QDs for BSA, BHb and Lyz were 0.1433, 0.1362 and 0.1124, the K_{SV} of NIP-coated QDs for BSA, BHb and Lyz were 0.1281, 0.1262 and 0.1121), indicating that there were no selective recognition sites in the NIP materials. Moreover, a series of ternary protein solutions of BSA/BHb/Lyz were prepared to study the competitive binding ability of the sensors. The re-binding was done by fixing the concentration of BSA and increasing the concentration of BHb and Lyz at the same time. As shown in Fig. 7(b), the fluorescence changes of BMIP-coated MWCNTs-QDs and BMIP-coated QDs were little affected by increasing the concentration of BHb and Lyz. These results imply the highly selective recognition ability of the BMIP-coated MWCNTs-QDs.

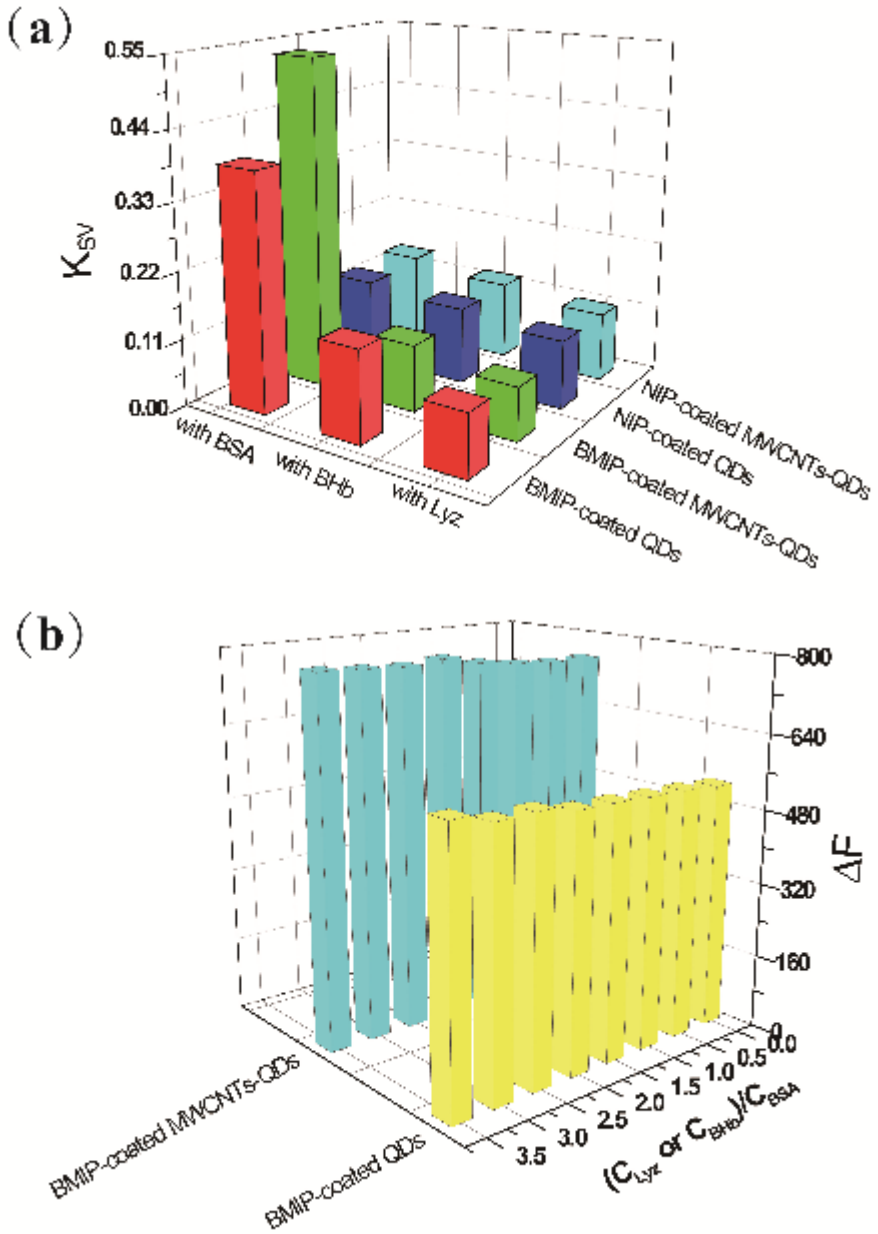

Fig. 7 (a) Quenching constant (K_{SV}) of BMIP-coated MWCNTs-QDs, BMIP-coated QDs, NIP-coated MWCNTs-QDs and NIP-coated QDs for BSA, BHb, and Lyz; (b) Effect of the competitive proteins BHb and Lyz on the binding of template protein BSA on the BMIP-coated MWCNTs-QDs and BMIP-coated QDs. Binding was done by fixing the concentration of BSA while increasing the concentration of BHb and Lyz at the same time. $\Delta F = F_0 - F$, here F_0 and F were the fluorescence intensities of the sensors in the absence and presence of the protein separately.

3.5 Detection range and limit of BMIP-coated MWCNTs-QDs

The BMIP-coated MWCNTs-QDs exhibited a distinctly linear decrease in fluorescence intensity with

the binding of the target protein in the concentration range of 5.0×10^{-7}-35×10^{-7} M. The linear relationship between F_0/F and Cq was observed with the regression equation $F_0 / F = 0.5348Cq + 0.9217$ (where Cq was in μM, R=0.9920). The limit of detection calculated as the concentration of BSA which quenched three times the standard deviation of the blank signal, divided by the slope of the standard curve, was 0.8×10^{-7}M. The precision for three replicate detections of 1.5×10^{-6} M BSA was 2.45% (relative standard deviation).

3.6 Possible fluorescence quenching mechanism of target protein on the biomimenic sensors

To understand the changes in fluorescence intensity due to target protein binding, the fluorescence quenching mechanism was investigated. In the current study, the recognition behaviors of the BMIP-coated QDs and BMIP-coated MWCNTs-QDs were studied *via* the changes of the fluorescence intensity based on the fluorescence quenching between BSA and these sensors. As revealed by the UV-vis absorption spectra in Fig. 8, the UV absorbance of BSA was close to the band gap, but further away from the emission spectrum of the BMIP-coated sensors. The charges of the conduction bands of the BMIP-coated sensors could transfer to the lowest unoccupied molecular orbital of BSA. The possible mechanism of energy transfer for the fluorescence quenching was excluded due to no spectral overlap between the absorption spectrum of the BSA and the emission spectrum of the sensors. From the above analysis we can conclude that electron transfer from the sensors to the protein was responsible for the mechanism of fluorescence quenching.[54]

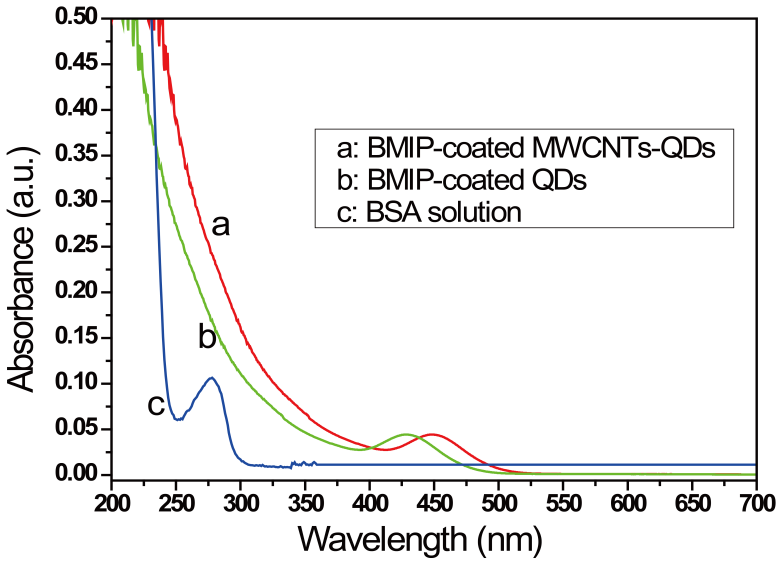

Fig. 8 UV-vis spectra of BMIP-coated MWCNTs-QDs (a), BMIP-coated QDs (b) and BSA solution (c).

4. Conclusions

We have developed a novel strategy to construct the MIP-based fluorescent sensor by combining the fluorescence superiority of CdTe/CdS QDs which were loaded on the surface of MWCNTs and the specific recognition of MIP. The introduction of MWCNTs has enhanced the template selectivity, fluorescence stability and mass-transfer efficiency of the sensor BMIP-coated MWCNTs-QDs towards target molecule BSA compared to BMIP-coated QDs without MWCNTs in the study. The novel biomimetic sensor obtained through this work may provide opportunities to develop a system that is efficient and effective and has potential in the design of highly effective synthetic fluorescent sensor for recognition of target protein.

Acknowledgments

This work was financially supported by the National Natural Science Foundation of China (21006010), Langsha Group, Jofo(WeiFang) Nonwoven Co. Ltd and the Fundamental Research Funds for the Central Universities.

References

AliBoucetta, H., Al-Jamal, K., McCarthy, D., Prato, M., Bianco, A., Kostarelos, K., 2008. Chem. Commun. 459-461.

Bossi, A., Piletsky, S.A., Piletska, E.V., Righetti, P.G., Turner, A.P.F., 2001. Anal. Chem. 73, 5281-5286.

Cesari, F., 2009. Nat. Rev. Mol. Cell Biol. 10, 577-577.

Chen, B.D., Zhang, H., Zhai, C.X., Du, N., Sun, C., Xue, J.W., Yang, D.R., Huang, H., Zhang, B., Xie, Q.P., Wu, Y.L., 2010. J. Mater. Chem. 20, 9895-9902.

Coombs, K.M., 2011. Expert. Rev. Proteomics 8, 659-677.

De Smet, D., Dubruel, P., Van Peteghem, C., Schacht, E., De Saeger, S., 2009. Food Additives and Contaminants Part A-Chemistry Analysis Control Exposure & Risk Assessment 26, 874-884.

Feazell, R.P., Nakayama-Ratchford, N., Dai, H.J., Lippard, S.J., 2007. J. Am. Chem. Soc. 129, 8438-8439.

Gao, D.M., Zhang, Z.P., Wu, M.H., Xie, C.G., Guan, G.J., Wang, D.P., 2007. J. Am. Chem. Soc. 129, 7859-7866.

Gill, R., Zayats, M., Willner, I., 2008. Angewandte Chemie International Edition 47, 7602-7625.

Holthoff, E.L., Bright, F.V., 2007. Acc. Chem. Res. 40,756-767.

Li, C., Ando, M., Sakai, E., Enomoto, H., Taguchi, T., Murase, N., 2011. Chem. Lett. 40, 258-260.

Li, H.B., Li, Y.L., Cheng, J., 2010. Chemistry of Materials 22, 2451-2457.

Li, L.L., Chen, D., Zhang, Y.Q., Deng, Z.T., Ren, X.L., Meng, X.W., Tang, F.Q., Ren, J., Zhang, L., 2007. Nanotechnology 18, 405102 (1-6).

Li, Q.W., Sun, B.Q., Kinloch, I.A., Zhi, D., Sirringhaus, H., Windle, A.H., 2006. Chem. Mater. 18, 164-168.

Lim, X.D., Zhu, Y.W., Cheong, F.C., Hanafiah, N.M., Valiyaveettil, S., Sow, C., 2008. ACS Nano 2, 1389-1395.

Liu, H.L., Fang, G.Z., Zhu, H.D., Li, C.M., Liu, C.C., Wang, S., 2013. Biosens. Bioelectron. 47, 127-132.

Liu, J.X., Yang, K.G., Deng, Q.L., Zhang, L.H., Liang, Z., Zhang, Y.K., 2011. Chem. Commun. 47, 3969-3971.

Liu, Z., Winters, M., Holodniy, M., Dai, H.J., 2007. Angew. Chem. Int. Ed. 46, 2023-2027.

Lucci, P., Derrien, D., Alix, F., Pérollier, C., Bayoudh, S., 2010. Anal. Chim. Acta 672, 15-19.

Matsui, J., Goji, S., Murashima, T., Miyoshi, D., Komai, S., Shigeyasu, A., Kushida, T., Miyazawa, T., Yamada, T., Tamaki, K., Sugimoto, N., 2007. Anal. Chem. 79, 1749-1757.

Pantarotto D., Singh R., McCarthy D., Erhardt M., Briand J., Prato M., Kostarelos K. Bianco A., 2004. Angew. Chem. Int. Ed. 43, 5242-5246.

Ravindran, S., Chaudhary, S., Colburn, B., Ozkan, M., Ozkan, C.S., 2003. Nano Lett 3, 447-453.

Shi, D.L., Guo, Y., Dong, Z.Y., Lian, J., Wang, W., Liu, G.K., Wang, L.M., Ewing, R.C., 2007. Adv. Mater. 19, 4033-4037.

Stinaff, E.A., Scheibner, M., Bracker, A.S., Ponomarev, I.V., Korenev, V.L., Ware, M., Doty, E.M.F., Reinecke, T.L., Gammon, D., 2006. Science 311, 636-639.

Tan, C.J., Chua, H.G., Ker, K.H., Tong, Y.W., 2008. Anal. Chem. 80, 683-692.

Tan, C.J., Tong, Y.W., 2007. Anal. Chem. 79, 299-306.

Wang, H.F., He, Y., Ji, T.R., Yan, X.P., 2009. Anal. Chem. 81, 1615-1621.

Whitcombe, M.J., Chianella, I., Larcombe, L., Piletsky, S.A., Noble, J., Porter, R., Horgan, A., 2011.

Chem. Soc. Rev. 40, 1547-1571.

Yuan, Z.M., Wang, J.R., Yang, P., 2013. Luminescence. 28, 169-175.

Zeng, Z., Hoshino, Y., Rodriguez, A., Yoo, H., Shea, K.J., 2010. ACS Nano 4, 199-204.

Zhang, W., Hea, X.W., Chen, Y., Li, W.Y., Zhang, Y.K., 2012. Biosens. Bioelectron. 31, 84-89.

Zhao, Y.J., Zhao, X.W., Tang, B.C., Xu, W.Y., Li, J., Hu, J., Gu, Z.Z., 2010. Adv. Funct. Mater. 20, 976-982.

Zhao, Y.Y., Ma, Y.X., Li, H., Wang, L.Y., 2012. Anal. Chem. 84, 386-395.